Preprints of the 21st IFAC World Congress (Virtual)
Berlin, Germany, July 12-17, 2020

A Novel Microsurgical Robot with Double-Parallelogram RCM Mechanism and Back-Driven Instrument Translation ⋆

Hsing-Chi Chen * **Wei-Jiun Su** ** **Cheng-Wei Chen** ***

* *Department of Electrical Engineering, National Taiwan University, Taipei, Taiwan (e-mail: r07921071@ntu.edu.tw).*
** *Department of Mechanical Engineering, National Taiwan University, Taipei, Taiwan (e-mail: weijiunsu@ntu.edu.tw).*
*** *Department of Electrical Engineering, National Taiwan University, Taipei, Taiwan (e-mail: cwchenee@ntu.edu.tw).*

Abstract: With the increasing demand for high-accuracy maneuvers in robot-assisted minimal invasive surgery (MIS), both the kinematic structure and the assembly errors of the microsurgical robot need to be improved. Traditionally, the insertion and retraction motion of the surgical tool is driven by a linear actuator mounted on the end-effector. However, this causes additional mass, inertia, and vibration. To mitigate this problem, a novel microsurgical robot with back-driven instrument translation is developed. Parameter optimization that considers the assembly errors of the double-parallelogram RCM mechanism is performed in the robot's mechanism design. A prototype of the design is fabricated and implemented. The experimental results validate the effectiveness of the proposed new mechanism.

Keywords: Microsurgical robots; Remote Center of Motion (RCM); double-parallelogram RCM mechanism; assembly error analysis; parameter optimization.

1. INTRODUCTION

Minimum invasive surgery (MIS) has the advantages of less bleeding, less pain, faster recovery, and smaller scars. However, it still faces many difficulties, such as limited dexterity, hand tremor, and vision deficiency. With the help of robotic technologies, delicate manipulations are enabled by applying tremor filtering, motion scaling, and force feedback [Prasad et al. (2004); Okamura (2009)]. These advanced techniques ensure precise and safe motion, reduce hand tremor, and therefore reduce the risks of inadequate operations during the surgical tasks.

The remote-center-of-motion (RCM) mechanism is widely used in the field of robot-assisted MIS. The RCM is a mechanical constrained virtual point in the space, at this very point it only allows the robot to perform rotary motion and prohibits the translational motion. Therefore, the RCM can be seen as an ideal point to be located at the surgical incision. Several RCM mechanisms have been proposed and well-studied. The most common type of the RCM mechanisms include circular arcs [Wilson et al. (2018); Yip et al. (2014)], double-parallelograms [Nisar et al. (2017); Li et al. (2014)], and spherical linkages [Kim et al. (2008); Lum et al. (2006)].

A common problem of these RCM mechanisms is about the actuation of the surgical tool's along insertion-retraction direction. Traditionally, the linear motion of the surgical instrument is actuated by a linear actuator placed at the end-effector. However, this results in larger inertia, extra mass, and undesired vibrations on the end-effector. To avoid these problems, the way of achieving the actuation of the tool insertion should be redesigned. A better method is moving the linear actuator from the end-effector to the base of the robot. However, it is difficult to implement this design concept when the RCM is achieved by circular arcs or spherical linkages mechanism. As a result, we will focus on the double-parallelogram RCM mechanism.

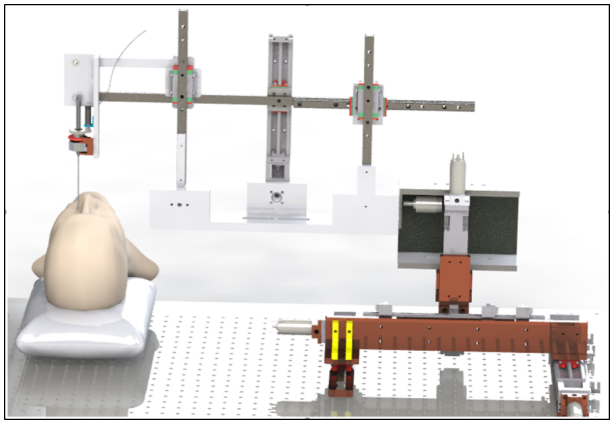

Fig. 1. The CAD model of the proposed microsurgical robot with double-parallelogram RCM mechanism and back-driven instrument translation.

Recent developments have shown possible designs that incorporate the double-parallelogram RCM mechanism and

⋆ This work was financially supported from the Young Scholar Fellowship Program by Ministry of Science and Technology (MOST) in Taiwan, under Grant MOST 108-2636-E-002-007.

back-driven translational motion. [Nisar et al. (2017)] used prismatic joints and an auxiliary parallelogram at the base to indirectly drive the insertion-retraction motion. This design creates additional joints and contacts, which lead to the amplification of assembly errors and increase the difficulty of implementation. Similarly, [Hadavand et al. (2014, 2011)] proposed an RCM mechanism which added one additional parallelogram at the base and used prismatic joints to convert the relative motion of the parallelograms into the linear motion of the end-effector. Because the translational motion of the tool is actuated by the relative motion of the two parallelograms, the nonlinear mapping between the geometry of parallelograms and linear motion results in the challenges of controlling the position and velocity of the tool.

In this paper, we propose an RCM mechanism which is capable of driving the insertion-retraction motion of the surgical tool from the back-side of the robot (Fig. 1). We revisit the design concept of the double-parallelogram RCM mechanism, and add additional prismatic joints on the rotary joints to allow for back-driven translational motion. In addition, a double-prismatic joint that constrains the excessive degree of freedom is included to sustain the double-parallelogram mechanism. The translational motion of the end-effector is linearly driven, thus it is easier to control the position and velocity of the tool. This design solves the problem of undesired vibrations and reduces the mass and inertia at the end-effector. Furthermore, the mechanism design is simple and with less joints and contacts, which enable high-precision motion after fabrication and implementation.

2. MECHANISM DESIGN

In this section, the design specifications of the microsurgical robot is depicted followed by the mechanism synthesis and kinematic analysis of the novel double-parallelogram RCM mechanism.

2.1 Design specifications

There are two essential requirements in robot-assisted MIS. First, the motion of the instrument must be constrained at the surgical incision. This can be achieved by applying RCM mechanisms in the robot design. Second, the robot must be able to manipulate within a desired workspace below the surgical incision.

Ophthalmic surgery is one of the most delicate microsurgery. In this paper, we are aiming at designing a microsurgical robot capable of performing precise motion within sufficiently large workspace required in ophthalmic surgery. The workspace requirement of robotic ophthalmic surgery is defined as in other literature [Hubschman et al. (2011)]:

(1) The pitch angle should cover from $-60^o \sim 60^o$ (as defined in Fig. 2(a), 0^o is vertical to ground)
(2) The yaw angle should cover from $25^o \sim 155^o$ (0^o towards the RCM)
(3) The instrument should be able to roll about its centerline.
(4) The insertion length should cover at least 50 mm stroke below the RCM point.

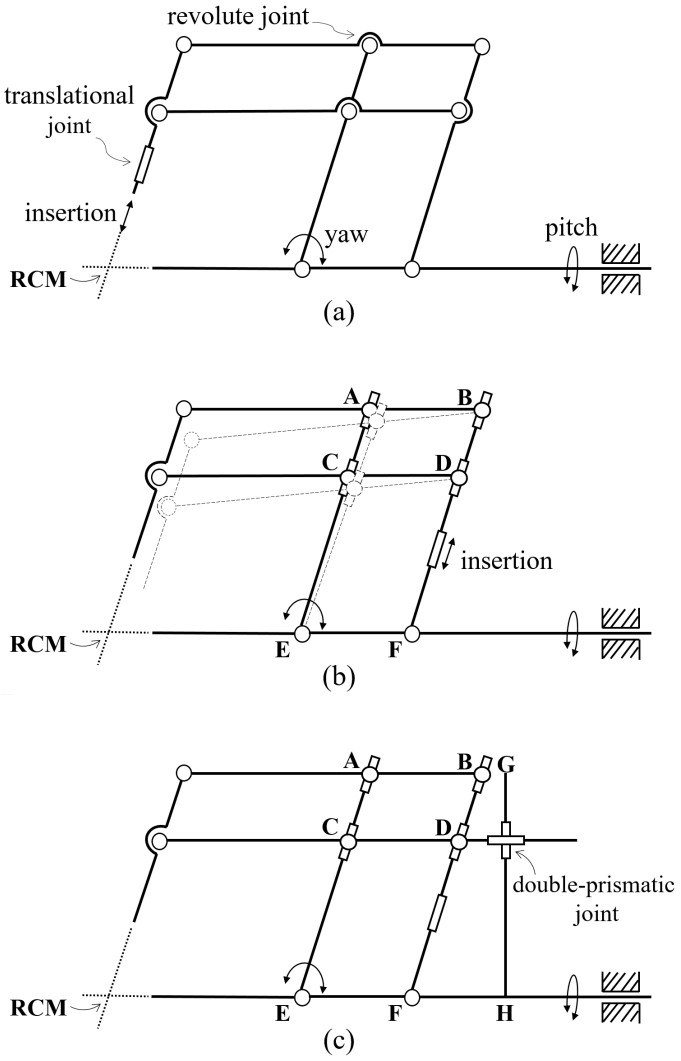

Fig. 2. The design concept of the novel back-driven double-parallelogram RCM mechanism. (a) The conventional design. (b) The instrument translation is moved to the back-side, which necessitates the translational degree of freedom at A and C joint, and therefore voids the RCM mechanism. (c) Back-driven instrument translation constrained by a double-prismatic joint to ensure the RCM mechanism.

2.2 Mechanism Synthesis

Fig. 2(a) shows a basic double-parallelogram RCM mechanism. Based on this basic one, we remove the linear actuator at the end-effector and put it at the back-side of the robot. To drive the tool translational motion, we augment prismatic joints at the revolute joints at A, B, C, and D, as the mechanical structure illustrated in Fig. 2(b). The linear actuator applied on DF drives the translational motion of the end-effector and provides linear position and velocity motion mapping. However, the prismatic joints create an excessive degree-of-freedom along AC direction, which voids the double-parallelogram RCM mechanism. The links CD and EF might not remain parallel all the time (as illustrated by the dotted lines in Fig. 2(b)). This is why the RCM is no longer effective.

To avoid this problem, we add an auxiliary linkage GH which attaches a double-prismatic joint. The double-prismatic joint slides freely on GH and CD, thus it ensures CD to be parallel to EF all the time (see Fig. 2(c)). Because the link GH and the double-prismatic joint are implemented for the use of guaranteeing AB and CD to be parallel with EF, the link CE is no longer necessary in achieving the RCM mechanism. The link CE can be removed, so as the links of AB and BD. However, for the stiffness of the robot manipulator, we still keep these links in our prototypical design.

2.3 Kinematics and Dynamics Analysis

The designed mechanism is shown as Fig. 3, where the related coordinates are attached for the kinematics analysis. The actuated joints include θ_1, θ_2, and θ_3 which represents the pitch, yaw, and roll angle, respectively. In addition, the instrument insertion and retraction d is actuated by a linear actuator. When d increases, the tool retracts from the RCM; when d decreases, the tool inserts through the RCM and enters the workspace. Based on the Denavit-Hartenberg convention, the forward kinematics of this robot is derived as

$$ {}^{7}_{0}\mathbf{T} = \begin{bmatrix} R & T \\ 0 & 1 \end{bmatrix} \tag{1} $$

where

$$ R = \begin{bmatrix} c_1c_2c_3 + s_1s_3 & s_1c_3 - c_1c_2s_3 & -c_1s_2 \\ s_1c_2c_3 - c_1s_3 & -c_1c_3 - s_1c_2s_3 & -s_1s_2 \\ -s_2c_3 & s_2s_3 & -c_2 \end{bmatrix} \tag{2} $$

$$ T = \begin{bmatrix} c_1s_2(d-P) \\ s_1s_2(d-P) \\ c_2(d-P) + (l_1 + l_2) \end{bmatrix} \tag{3} $$

where $c_i := \cos(\theta_i)$, $s_i := \sin(\theta_i)$. By calculating the Jacobian matrix, the singular points of the double-parallelogram RCM mechanism can be determined as:

$$ \begin{cases} \theta_2 = 0, \pi \\ d = P \end{cases} \tag{4} $$

The case of $d = P$ indicates that the tool-tip of the instrument is exactly pointing at the RCM. Therefore, this singularity is obtained as desired. Besides, the manipulability w of this mechanism is defined as Eq.5 [Yoshikawa (1985)]:

$$ w = |-s_2(d-P)^2| \tag{5} $$

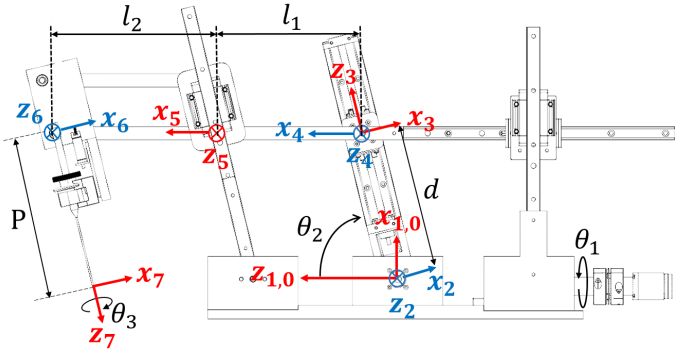

Fig. 3. The prototype of the microsurgical robot attached with the definitions of coordinates and parameters.

3. MECHANISM OPTIMIZATION

In this section, we analyze the effect of possible mechanical and geometric errors to the tool-tip positioning accuracy. This analysis leads to the optimization of the design parameters.

3.1 Assembly Error Analysis

The kinematic error of the double-parallelogram RCM mechanism is contributed to the manufacturing errors and the assembly errors. The manufacturing errors are usually in the level of $\pm$ 50 μm, which is relatively smaller than the assembly errors. Therefore, here we will focus on the effect of assembly errors on the tool-tip positioning accuracy.

There are several kind of assembly errors may have significant effects towards the positioning accuracy. Specifically, we will analyze the effects of inaccurate parallelogram (as the angle α in Fig. 4), misalignment of pitch angle actuation and surgical instrument (as the γ and ϵ shown in Fig. 5).

(1) Inaccurate parallelogram α : α comes from the assembly error of the double-prismatic joint. To achieve a mechanical constrained RCM, CD and EF must be parallel to each other. However, when α is not exactly 0 degrees, i.e., CD is not orthogonal to GH and therefore CD is not parallel to EF, the RCM is no longer existing, resulting in inaccurate tool-tip positions.

As shown in Fig. 4, the length of d is fixed, so as the link length of CD and EF. Hence, non-zero α moves the joint C and creates an offset angle β. As a result, the angle $\angle ECD = \theta_2 + \beta$ is different from $\angle EFD = \theta_2$. Thus, CDEF is no longer a parallelogram in this situation. β can be determined as a function of d, θ_2, and α,

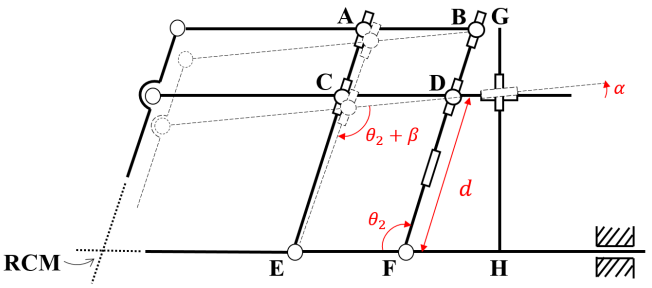

Fig. 4. The geometry of assembly error caused by the non-orthogonal constraint between CD and GH segments.

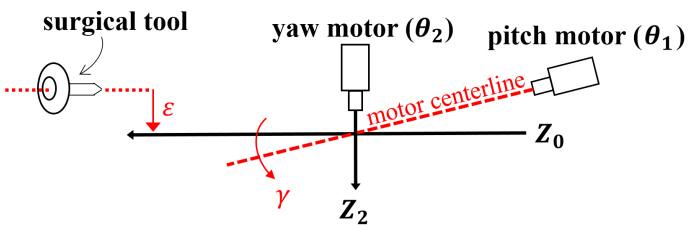

Fig. 5. The geometry of assembly error caused by the misalignment between the robot and the actuator.

$$\beta = sin^{-1}(\frac{a}{b}s_{(\pi-\theta_2-\alpha)}) - \theta_2 \tag{6}$$

where

$$a = \sqrt{l_1^2 + d^2 - 2l_1 d c_2} \tag{7}$$

$$b = \sqrt{l_1^2 + a^2 - 2l_1 a c_{(\pi-\theta_2-\alpha)}} \tag{8}$$

and the tool-tip position of the end-effector considering a non-zero α is

$$\begin{bmatrix} x \\ y \\ z \end{bmatrix} = \begin{bmatrix} c_1(ds_2 - Ps_{\beta-\alpha} - (l_1+l_2)s_\alpha) \\ s_1(ds_2 - Ps_{\beta-\alpha} - (l_1+l_2)s_\alpha) \\ c_2 d - P(c_\alpha c_\beta + c_\delta c_\beta) + c_\alpha(l_1+l_2) \end{bmatrix} \tag{9}$$

Note that here we only present the tool-tip position. By calculating the forward kinematics and comparing with the ideal forward kinematics, both the position and orientation errors are affected by the assembly error of α.

We can observe that in the x and y direction the term $(l_1+l_2)s_\alpha$ might be an influential term for the positioning error, as the length of (l_1+l_2) is usually large.

(2) Actuator misalignment γ : The assembly error of γ is caused by the connector between the pitch motor and the Z_0 shaft of the double-parallelogram mechanism (Fig. 5). Since the entire robot is seated on Z_0 shaft, this error may stack up and degrade the tool-tip positioning accuracy. The tool-tip position of the end-effector considering a non-zero γ is derived as

$$\begin{bmatrix} x \\ y \\ z \end{bmatrix} = \begin{bmatrix} c_1 s_2(d-P) - s_1 s_\gamma(c_2(d-P) + l_1 + l_2) \\ s_1 s_2(d-P) + c_1 s_\gamma(c_2(d-P) + l_1 + l_2) \\ c_\gamma(c_2(d-P) + l_1 + l_2) \end{bmatrix} \tag{10}$$

Again, the positioning error grows as the length of (l_1+l_2) increases.

(3) Instrument misalignment ϵ : ϵ is caused by the misalignment between Z_0 shaft and the surgical tool's centerline (Fig. 5). Ideally, the surgical instrument and Z_0 shaft should intersect. The intersection is noted as the RCM. If the alignment is not addressed well, the RCM will loss.

The tool-tip position of the end-effector considering a non-zero ϵ is

$$\begin{bmatrix} x \\ y \\ z \end{bmatrix} = \begin{bmatrix} c_1 s_2(d-P) - \epsilon * s_1 \\ s_1 s_2(d-P) + \epsilon * c_1 \\ (c_2(d-P) + l_1 + l_2 \end{bmatrix} \tag{11}$$

Apparently, the tool-tip positioning error only depends on ϵ and θ_1. The scale of it is not affected by other kinematic parameters such as the length of (l_1+l_2).

In order to understand the effect of the abovementioned assembly errors, in Fig. 6 it shows the path of the tool-tip when the robot is tracking a circle. The positioning error caused by different assembly errors has a certain distortion pattern. This information is useful in the calibrating procedure. Fig. 7 shows the root-mean-square error of the tool-tip positions when the assembly errors increase. This error is computed at the position where $d = P$ (Fig. 3), meaning the tool-tip is exactly pointing at the RCM. From both Fig. 6 and Fig. 7, we can see α is the most influential assembly error.

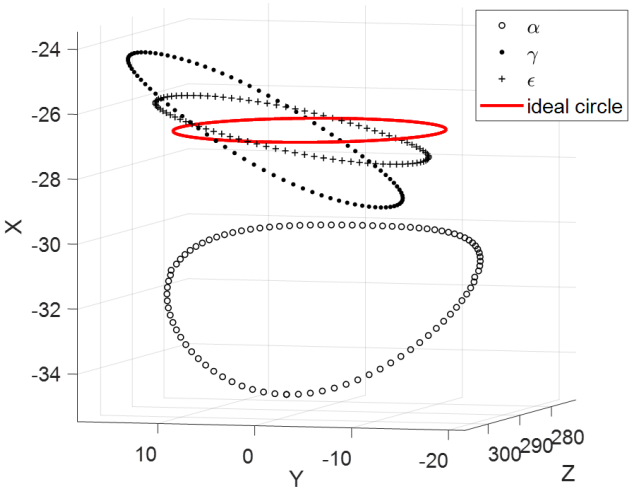

Fig. 6. The simulated circle path with respect to different assembly error, where α and γ are both set as 1^o; ϵ is 2 mm.

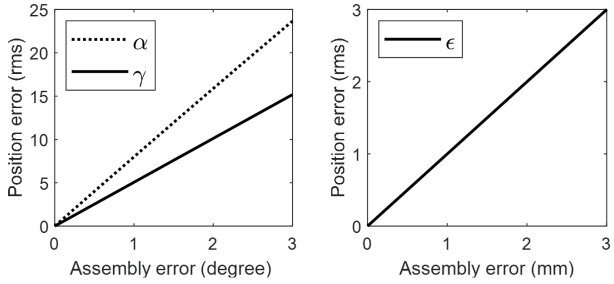

Fig. 7. The tool-tip positioning error versus assembly error. (a) The positioning RMS error per α and γ. (b) The positioning RMS error per ϵ.

Although α is more prone to the positioning error at the end-effector, it is relatively easier to calibrate this error because CD and GH links are directly connected through the double-prismatic joint. On the other hand, it is more difficult to ensure the assembly error of γ is sufficiently small, because Z_0 shaft supports the entire robot and suffers from gravity. Therefore, it is important to consider the assembly error of γ when designing the robot's kinematic parameters.

3.2 Mechanism Optimization

In the design stage, we need to determine critical kinematic parameters of the robot such as the linkages' length. A cost function is defined, which optimizes the performance of the robot in terms of manipulability and accuracy.

(1) *Manipulability*: Manipulability indicates how well the robot can be manipulated in any direction. From Eq. 2 we can compute the manipulability at a specific configuration of θ_2 and insertion d. However, we usually care more about the average performance, as shown in Eq. 13. Note the term A is used to compute an average value but has no physical effect on the optimization of the cost function.

$$\frac{1}{A}\int_{\theta_2}\int_{d} |s_2(d-P)^2| \mathrm{d}\theta_2 \mathrm{d}d \tag{12}$$

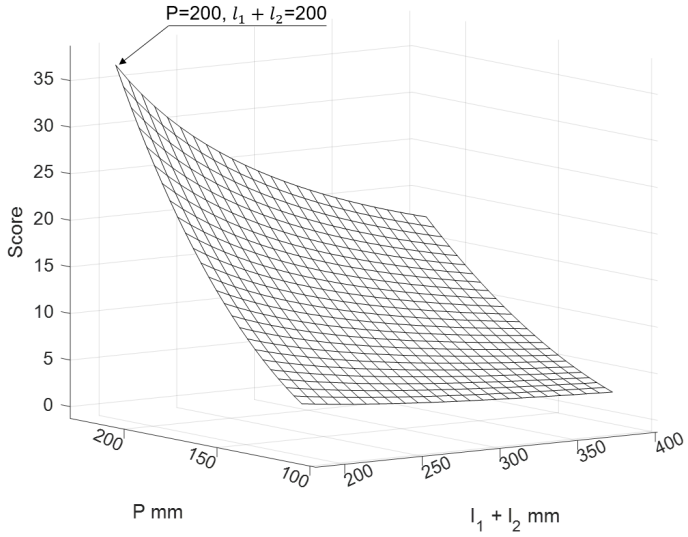

Fig. 8. The scores of the cost function at different design parameters. This results indicate that lager P and smaller $l_1 + l_2$ optimizes the mechanism design.

(2) *Reducing assembly errors*: As for the robot's accuracy, we took the result of the assembly error analysis as our design consideration. For the error of γ, the term $c_2(d-P)+l_1+l_2$ exists in both of the x and y axis in Eq. 10. Therefore, the average of this term is taken as the penalty:

$$\int_{\theta_2}\int_{d}|\frac{1}{c_2(d-P)+l_1+l_2}|\mathrm{d}\theta_2\mathrm{d}d \tag{13}$$

After combining Eq. 12 and Eq. 13, the cost function is defined as

$$\max_{l_1+l_2,P}\int_{\theta_2}\int_{d}|\frac{s_2(d-P)^2}{c_2(d-P)+l_1+l_2}|\mathrm{d}\theta_2\mathrm{d}d \tag{14}$$

The optimization result in Fig. 8 shows that with higher P and lower $l_1 + l_2$, higher optimization score can be obtained. Thus the P is chosen to be 200 mm. Considering the workspace requirement, $l_1 + l_2$ is chosen as 290 mm which is the minimum length without interfering within the desired workspace.

4. EXPERIMENTAL RESULTS

A prototypical microsurgical robot based on the proposed design concept and mechanism optimization was fabricated and assembled. The actuation of the pitch and yaw angle are both driven by DC servo motors (Faulhaber Micromotors 2657W024CR with 30/1-134:1 Gearhead). The insertion length is actuated by the single-axis ball screw linear slider (Hiwin KK4001) with travelling range of 175 mm driven by a DC servo motor (Faulhaber Micromotors 2642W024CR). The output position of each actuator is measured from the optical encoder (Faulhaber Micromotors IE3-1024). The control of the DC servo motors is conducted by a typical PID control method with the control sampling rate of 1 kHz.

We first evaluated whether the workspace requirement defined in Sec. 2.1. was met. When the instrument was inserted 50 mm below the RCM, the pitch angle θ_1 was able to move from -75^o to 70^o degrees; the yaw angle θ_2 was able to move from 21^o to 157^o degrees. Both of them were shown larger than the required motion range.

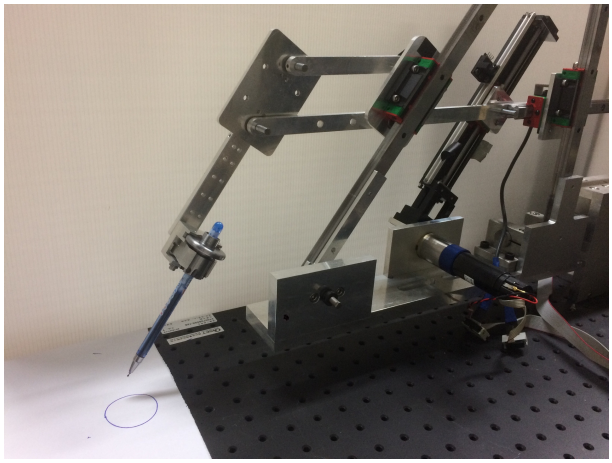

Fig. 9. The experiment setup of the microsurgical robot, which was manipulated to draw a circle.

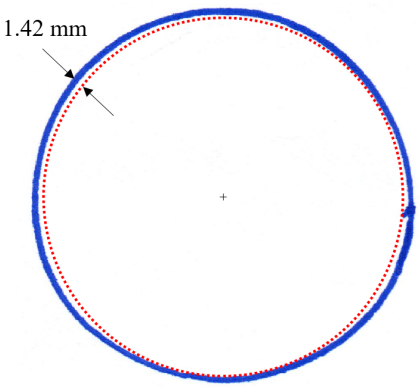

Fig. 10. An example of the circle drawn by the microsurgical robot (solid line). The roundness of the circle was 0.93, and the maximum error (to the reference, dash line) is about 1.42 mm.

To evaluate the tool-tip positioning accuracy, the robot was commanded to draw a circle. The experimental setup is shown in Fig. 9. Due to the effect of assembly errors, a rough calibration procedure was conducted such that the plane of the drawn circles would align with the paper, otherwise the pen might collide with the table where the paper was attached. Interestingly, this calibration process also guided us to know which assembly error contributed the most to the tool-tip positioning error.

One of the circle drawn by this prototype is shown in Fig. 10. The roundness of this circle, 0.93, was calculated [Cox (1927)] by

$$roundness \triangleq \frac{4\pi \cdot Area}{Perimeter^2} \tag{15}$$

We also measured the maximum error, which represents the maximum distance between the drawn circle and the commanded reference. The experimental results are listed in Table 1, which shows the roundness and maximum error calculated from each drawn circle. The average roundness of the drawn circles was 0.93, while a "perfect" circle had

Table 1. The experimental results. Note that the roundness of a "perfect" circle was measured to be 0.98 by the image processing algorithm.

Circle	Roundness	Max. Error
1	0.92	1.44 mm
2	0.93	1.42 mm
3	0.93	1.48 mm
4	0.92	1.50 mm
5	0.93	1.55 mm
6	0.93	1.55 mm
7	0.92	1.50 mm
8	0.93	1.63 mm
9	0.94	1.53 mm
Mean	0.93	1.51 mm
Standard deviation	0.0060	0.0967 mm

the roundness of 0.98 in our image processing algorithm. The maximum errors in the 9 repeated experiments were all less than 2 mm, which indicates that this prototype has the potential to be applied in robot-assisted microsurgery. We believe the positioning accuracy can be further improved after properly calibrating the assembly errors.

5. CONCLUSION

A novel RCM mechanism is proposed for back-driven tool insertion and retraction. The proposed mechanism redesigns the double-parallelogram RCM mechanism. The rotary joints that connect the two parallelograms are augmented with prismatic joints, therefore the translational motion of the tool can be driven remotely. This design solves the issues of large inertia, floating mass, and unwanted vibrations when the tool translation is driven by a linear actuator mounted on the end-effector. The parametric optimization and possible assembly errors of the proposed RCM mechanism are analyzed. This helps the mechanism design in achieving the desired workspace and meanwhile minimizing the potential tool-tip positioning inaccuracy. In addition, the results of assembly error analysis could also be used to assist the mechanical calibration process. A prototype of this design has been implemented and shown the potential to be applied in high-accuracy robot-assisted microsurgery. In our future research, we will focus on reducing the error of the prototype and developing a more compact strategy for assembly error analysis and calibration.

REFERENCES

Cox, E. (1927). A method of assigning numerical and percentage values to the degree of roundness of sand grains. *Journal of Paleontology*, 1(3), 179–183.

Hadavand, M., Mirbagheri, A., Behzadipour, S., and Farahmand, F. (2014). A novel remote center of motion mechanism for the force-reflective master robot of haptic tele-surgery systems. *The International Journal of Medical Robotics and Computer Assisted Surgery*, 10(2), 129–139.

Hadavand, M., Mirbagheri, A., Salarieh, H., and Farahmand, F. (2011). Design of a force-reflective master robot for haptic telesurgery applications: Robomaster1. In *2011 Annual International Conference of the IEEE Engineering in Medicine and Biology Society*, 7037–7040. IEEE.

Hubschman, J., Son, J., Allen, B., Schwartz, S., and Bourges, J. (2011). Evaluation of the motion of surgical instruments during intraocular surgery. *Eye*, 25(7), 947.

Kim, S.K., Shin, W.H., Ko, S.Y., Kim, J., and Kwon, D.S. (2008). Design of a compact 5-dof surgical robot of a spherical mechanism: Cures. In *2008 IEEE/ASME International Conference on Advanced Intelligent Mechatronics*, 990–995. IEEE.

Li, J., Zhang, G., Xing, Y., Liu, H., and Wang, S. (2014). A class of 2-degree-of-freedom planar remote center-of-motion mechanisms based on virtual parallelograms. *Journal of Mechanisms and Robotics*, 6(3), 031014.

Lum, M.J., Rosen, J., Sinanan, M.N., and Hannaford, B. (2006). Optimization of a spherical mechanism for a minimally invasive surgical robot: theoretical and experimental approaches. *IEEE Transactions on Biomedical Engineering*, 53(7), 1440–1445.

Nisar, S., Endo, T., and Matsuno, F. (2017). Design and kinematic optimization of a two degrees-of-freedom planar remote center of motion mechanism for minimally invasive surgery manipulators. *Journal of Mechanisms and Robotics*, 9(3), 031013.

Okamura, A.M. (2009). Haptic feedback in robot-assisted minimally invasive surgery. *Current opinion in urology*, 19(1), 102.

Prasad, S.M., Prasad, S.M., Maniar, H.S., Chu, C., Schuessler, R.B., and Damiano Jr, R.J. (2004). Surgical robotics: impact of motion scaling on task performance. *Journal of the American College of Surgeons*, 199(6), 863–868.

Wilson, J.T., Gerber, M.J., Prince, S.W., Chen, C.W., Schwartz, S.D., Hubschman, J.P., and Tsao, T.C. (2018). Intraocular robotic interventional surgical system (iriss): Mechanical design, evaluation, and master–slave manipulation. *The International Journal of Medical Robotics and Computer Assisted Surgery*, 14(1), e1842.

Yip, H.M., Li, P., Navarro-Alarcon, D., Wang, Z., and Liu, Y.h. (2014). A new circular-guided remote center of motion mechanism for assistive surgical robots. In *2014 IEEE International Conference on Robotics and Biomimetics (ROBIO 2014)*, 217–222. IEEE.

Yoshikawa, T. (1985). Manipulability of robotic mechanisms. *The international journal of Robotics Research*, 4(2), 3–9.